Photoproduction of ϕ Mesons with Linearly Polarized Photons

D.J. Tedeschi,*[†‡] S.A. Dytman, J.A. Mueller*
University of Pittsburgh, Pittsburgh, PA 15260

P.L. Cole,* B.L. Berman, W.J. Briscoe, K.S. Dhuga
Center for Nuclear Studies
The George Washington University, Washington, DC 20052

C.E. Keppel, R.A. Williams
Hampton University, Hampton, VA 23668

H. Funsten
College of William and Mary, Williamsburg, VA 23185

H. Crannell, D.I. Sober
The Catholic University of America, Washington, DC 20064

R. Ent, F.J. Klein, J.H. Mitchell, E.S. Smith
Thomas Jefferson National Accelerator Facility, Newport News, VA 23606

&

The CLAS Collaboration

November 20, 1997

---

*Spokesperson
[†] Contact-person
[‡] Will present proposal

Abstract

We propose to measure the reaction $\vec{\gamma} + p \rightarrow p + \phi$ with $\phi \rightarrow K^+K^-$ in the photon energy range of $1.9 < E_\gamma < 2.2$ GeV by tagging the incident photon energy and detecting the final-state proton in coincidence with the decay K^+ in the CLAS detector. The photons will be produced by coherent bremsstrahlung from a 4 GeV (6 GeV) electron beam incident on a diamond radiator, and will provide an average polarization of 65% (80%). The proposal to build the Coherent Bremsstrahlung Facility has been approved. The reaction can be completely specified by 12 complex density matrix elements composed of 17 independent, real functions of which 11 are measureable. The use of a linearly polarized beam of photons will allow for the extraction of nine of these functions by measuring the angular distributions of the decay kaons for each value of the 4-momentum transfer squared (t). The maximum value of t is -2.0 (GeV/c)^2 and the experiment will obtain data with good statistics up to about -1.2 (GeV/c)^2. The evolution of these density matrix elements as a function of t will quantify the contributions to the production amplitude due to either diffractive scattering or pseudo-scalar meson exchange. Presently existing data from a bubble-chamber experiment are consistent with diffractive scattering but have poor statistical accuracy. If either the diffractive mechanism or the pseudo-scalar meson exchange dominates the cross section, we expect that all but two of these nine density matrix elements will be identically equal to zero. Significant departure of any of the other seven quantities from zero will indicate new production channels. We ask for 500 hours of beam time (100 hours with 4 GeV beam and the rest at 6 GeV) that should be contiguous with the time already approved for experiment E94-109 in the $\gamma 8$ CLAS run period.

1 Introduction

Understanding the processes involved in the photoproduction of vector mesons is an important part of the CEBAF program, touching physics issues of vector meson dominance (VMD), the strangeness content of the nucleon, and t-channel meson exchange (including π, η, and η') processes [1]. The presently existing data are of poor statistical accuracy and only the VMD or diffractive signature is clearly visible. In the CEBAF experiments, the goals are to go well beyond this single issue and measurements involving polarization will be a key part of the advance. We will measure the photoproduction of ϕ mesons from the proton by using a linearly polarized beam of photons together with the complete $\phi \to K^+K^-$ decay distribution.

Although diffractive scattering is expected to dominate at low 4-momentum transfer squared (t) and high energies, this mechanism alone will be insufficient for a complete description of ϕ meson production near threshold. For c.m. energies near ϕ-photoproduction threshold, π and η meson exchange are expected to contribute significantly to the cross section, as well as processes which violate the Okubo-Zweig-Iizuka (OZI) rule. The OZI rule states that hadronic decays and Yukawa couplings between states with no common flavors, i.e. disconnected quark graphs, are suppressed. A model calculation [2] including both pomeron-exchange (a $J^\pi = 0^+$ exchange that was introduced to describe the diffractive nature of the presently existing data) and pseudo-scalar meson exchange ($J^\pi = 0^-$) for the energy range of the proposed experiment is shown in Figs. 1 and 2. Whereas diffractive scattering is intrinsically a *natural* parity exchange, pseudo-scalar meson exchange possesses the quantum numbers of the *unnatural* parity process. However, the existing total and differential cross-section data are too sparse to draw any further conclusions on the nature of the parity exchange at threshold energies [3].

There is considerable theoretical interest in the strangeness content of the proton and the nature of OZI violating processes [1]. Deep inelastic scattering [4] and the 'sigma term' from π-nucleon scattering [5] have provided evidence that $s\bar{s}$ pairs in the nucleon contribute to observable quantities. Near the ϕ meson production threshold, direct knockout of a pre-existing $s\bar{s}$ pair in the proton [6, 7] and π+η-meson exchange are predicted to have cross sections comparable with the diffractive process [2, 8]. However, very few data exist for the photoproduction of ϕ mesons, and the data which have been published are consistent with diffractive scattering in the vector meson dominance model.

The results of model calculation [8] which includes pomeron (0^+) and meson exchange (π, η), as well as effective $s\bar{s}$ knock-out and OZI evading processes (ϕNN) is shown in Figs. 3 and 4. The two versions of this model differ in the treatment of the threshold behavior of the pomeron process. Note that the different versions of the model contain different t dependencies, and that cross section data alone cannot distinguish between them. Both diffractive scattering and one-pion exchange processes are strongly forwardly peaked. Measuring the nine density matrix elements as a function of four-momentum transfer squared near the ϕ meson production threshold will provide the opportunity for disentangling the competing parity exchange mechanisms, and may give an indication of new physics.

The quantities to be measured in this experiment are the spin density matrix elements of the photoproduced ϕ meson. These observables, three from unpolarized photoproduction experiments and six additional ones with a linearly polarized beam of photons [9], are extracted in the rest frame of the ϕ meson by measuring the polar and azimuthal angular distributions of the decay kaons. Knowledge of the direction of polarization of the beam of linearly polarized photons will serve as a parity filter to distinguish between natural and unnatural parity exchange [10, 11]. Of these nine quantities, all but two will be identically equal to zero if the photoproduction of the ϕ meson is mediated by either pomeron or pseudo-scalar exchange. Opposite values are expected for these two processes and a direct measurement will allow one to readily distinguish between contributions from natural and unnatural parity exchange. Of the other seven spin density matrix elements, a significant departure from zero will signal contributions from previously unmeasured production mechanisms.

We therefore are proposing an experiment to measure the reaction $\vec{\gamma} p \to p\phi$ using a probe of linearly polarized photons and measuring the yield products in the CEBAF Large Acceptance Spectrometer (CLAS). The CLAS detector, along with a polarized photon beam (using the recently approved Coherent Bremsstrahlung Facility), provides the unique opportunity to measure the small ϕ-meson production cross section to high accuracy over a large range of angles. In this experiment we propose to study the reaction $\gamma + p \to p + \phi \;\; (\phi \to K^+K^-)$ by detecting the proton and the decay K^+ in the CLAS, and measuring the angular distributions of the K^+ as a function of t. A tightly collimated beam of tagged photons with energies in the range of $1.9 < E_\gamma < 2.2$ GeV and average polarization of 65% (80%) will be produced by coherently scattering a 4 GeV (6 GeV) electron beam directed upon a thin diamond crystal radiator [12]. This beam will strike the 14 cm long Saclay liquid hydrogen target. With the measurement of the tagged photon, recoil proton, and the decay K^+ meson with CLAS, the reaction will be kinematically overdetermined; from the reconstruction of the missing 4-momentum of the decay K^-, we will determine the 4-momentum of the ϕ meson, as well as the angular distributions of the K^+ meson as a function of t.

2 Formalism

The primary goal of the experiment is to measure the angular distributions of the decay kaon resulting from the reaction $\vec{\gamma} p \to \phi p$ in the energy range of $1.90 \leq E_\gamma \leq 2.20$ GeV. Measurement of the decay angular distribution of the K^+ provides access to nine density matrix elements $\rho^\alpha_{\lambda,\lambda'}$ (and $|\rho^\alpha_{\lambda,\lambda'}| \leq 1$), which are formed of bilinear combinations of the helicity amplitudes. The subscripts refer to the helicity states of the ϕ meson in the helicity amplitudes and the superscript indicates the component of the Stokes vector describing the photon polarization [13]. For linearly polarized photons, $\vec{P_\gamma} = P_\gamma(\cos 2\Phi, \sin 2\Phi, 0)$, where P_γ is the magnitude of the photon beam polarization and Φ is the angle between the photon polarization vector and the production plane. Thus, $\rho^0_{1,-1}$ measures the interference of the ± 1 helicity states of the ϕ meson produced by unpolarized photons.

The decay kaon distribution describing the experiment proposed here can therefore be written as a sum of the unpolarized and linearly polarized components [9].

$$W^L(\cos\theta, \phi, \Phi) = W^0(\cos\theta, \phi) - P_\gamma \cos 2\Phi \; W^1(\cos\theta, \phi) - P_\gamma \sin 2\Phi \; W^2(\cos\theta, \phi) \qquad (1)$$

where

$$\begin{aligned} W^0(\cos\theta,\phi) &= \frac{3}{4\pi}[\frac{1}{2}(1-\rho^0_{00}) + \frac{1}{2}(3\rho^0_{00}-1)\cos^2\theta \\ &\quad -\sqrt{2}Re\,\rho^0_{10}\sin 2\theta\cos\phi - \rho^0_{1-1}\sin^2\theta\cos 2\phi] \qquad (2) \\ W^1(\cos\theta,\phi) &= \frac{3}{4\pi}[\rho^1_{11}\sin^2\theta + \rho^1_{00}\cos^2\theta \\ &\quad -\sqrt{2}\rho^1_{10}\sin 2\theta\cos\phi - \rho^1_{1-1}\sin^2\theta\cos 2\phi] \qquad (3) \\ W^2(\cos\theta,\phi) &= \frac{3}{4\pi}[\sqrt{2}Im\,\rho^2_{10}\sin 2\theta\cos\phi - Im\,\rho^2_{1-1}\sin^2\theta\cos 2\phi] \qquad (4) \end{aligned}$$

All angles and density matrix elements are defined in the rest frame of the ϕ meson with the z-axis opposite the outgoing proton momentum (*helicity frame*). The angles θ and ϕ are the polar and azimuthal angles of the decay kaon (K^+) in this system. The angle Φ is the angle between the photon polarization vector and the cms production plane (see Fig. 5).

Parity relations constrain the nine density matrix elements and provide insight into the underlying physics. The amount of natural or unnatural parity that is exchanged in the t-channel process is a characteristic of the exchange mechanism. The exchange of pseudoscalar mesons implies unnatural parity ($J^\pi = 0^-$) while the exchange of pomeron carries natural parity ($J^\pi = 0^+$). A determination of the density matrix elements will quantify the amount of natural and unnatural parity exchange [9]. For example,

$$\rho^1 = \rho^{1(N)} + \rho^{1(U)} \qquad (5)$$

$$\rho^{1(N/U)}_{1-1} = \rho^1_{1-1} \pm \frac{1}{2}(1-\rho^0_{00}) \qquad (6)$$

The plus or minus sign refer to natural or unnatural parity exchange, respectively. The parity asymmetry to the total cross section can then be expressed as,

$$P_\sigma = \frac{\sigma_N - \sigma_U}{\sigma_N + \sigma_U} = 2\rho^1_{1-1} - \rho^1_{00} \qquad (7)$$

If the production mechanisms carry only natural parity, then $P_\sigma = 1$ which implies $\rho^1_{1-1} = 0.5$ and $\rho^1_{00} = 0$. $P_\sigma = -1$ indicates unnatural parity exchange and the density matrix element ρ^1_{1-1} will have opposite sign. An intermediate value can then be decomposed into its constituent contributions from the sum of these processes.

The beam asymmetry, as measured in previous experiments where the photon polarization vector is either parallel or perpendicular to the production plane with $\phi = \pi/2$ and $\Phi = 0(\|)$ or $\Phi = \pi/2(\perp)$ is defined as

$$\Sigma = \frac{\sigma_\| - \sigma_\perp}{\sigma_\| + \sigma_\perp} = \frac{\rho^1_{11} + \rho^1_{1-1}}{\rho^0_{11} + \rho^0_{1-1}} \qquad (8)$$

If helicity is conserved in the s channel, then there are only two nonzero density matrix elements – $\rho^1_{1-1} = 0.5$ and $Im\ \rho^2_{1-1} = -0.5$. This leads to the prediction that $\Sigma = 1.0$. Any significant deviation from unity is a strong indication that mechanisms other than diffraction are present. Calculations for the asymmetry parameter are shown shown in Figs. 6 and 7. At low-t the predicted asymmetry (solid line) depends on the amount of pseudoscalar exchange while at larger t the OZI evading amplitudes (ϕNN) affect the asymmetry.

2.1 Previous Measurements

There are only three previous measurements using polarized photons. The asymmetry parameter has been measured by these groups and the results are tabulated in Table 1 [14, 15]. The results of [16] are not included due to the high background contamination in their published result [3]. The results of the remaining two groups differ, but may not be inconsistent with each other because of the limited statistics and differing theoretical expectations for different regions in $\sqrt{s}$. The Halpern group detected 379 ϕ mesons and the Ballam group only 114. The angular distributions from ref. [15] are shown in Fig. 8.

There are also indications of contributions from processes other than diffraction in published unpolarized data. The differential cross section for ϕ photoproduction with photon energy $2.8 < E_\gamma < 3.8$ GeV is shown in Figure 9. [17]. The structure at $t = -0.4$ (GeV/c)^2 and the change in slope at larger t may not be the result of diffractive scattering, however, because the experiment was performed with unpolarized photons, the analysis was unable to distinguish different production mechanisms and thus concluded consistency with diffraction.

E_γ (GeV)	$\|t\|$ (GeV/c)^2	Σ	Reference
2.8 - 4.7	0.02 - 0.8	0.25 ± 0.35	Ballam
8.14	0.2	0.985 ± 0.12	Halpern
9.3	0.02 - 0.8	0.72 ± 0.6	Ballam

Table 1: Previous ϕ meson asymmetry (Σ) measurements.

For high photon energy and low 4-momentum transfer squared, the diffractive process dominates and a value of Σ consistent with unity as measured by Halpern et al. is not surprising. For photon energies below 3 GeV, meson exchange or other effects may account for a dilution of the asymmetry. The energy dependence of meson exchange could be responsible for the energy dependence of the asymmetry seen by Ballam. The data are too limited in statistics, however, to draw any further conclusions on or elucidate the nature of the t dependence of the asymmetry.

2.2 Approved Hall B ϕ Meson Experiments

Our proposed experiment complements the two approved Hall B ϕ meson production experiments. Table 2 contains a comparison of the kinematics covered. Experiment E93-022 will study the unpolarized electroproduction of the ϕ meson [21]. The density matrix elements will be measured as a function of Q^2 in the effort to separate the pseudo-scalar exchange from the diffractive contributions. In the search for hidden color effects, experiment E93-031 will measure the photoproduction of ϕ mesons at higher energies [22] using unpolarized photons.

Our proposed experiment will constrain the density matrix elements at the $Q^2 = 0$ point in the same energy range as E93-022. Our experiment, furthermore, differs from E93-031 in that we will measure the ϕ meson photoproduction near threshold and at lower t employing a linear polarized beam of photons as our probe; thus providing a complementary (low-t) measurement of the pomeron contribution to ϕ meson production. We are already collaborating closely with E93-022 and E93-031 on common analysis issues such as acceptance, background, and detection efficiency.

Experiment	Beam Type	CMS Energy (GeV)	t $(\mathrm{GeV}/c)^2$
E93-022	electron	$2.0 < W < 2.3$	$-1.8 < t < -0.2$
E93-031	incoherent brems. γ	$\sqrt{s} > 2.5$	$-5.0 < t < -1.0$
proposal	coherent brems. γ	$2.11 < \sqrt{s} < 2.24$	$-1.2 < t < -0.2$

Table 2: Parameters of ϕ meson experiments with CLAS.

3 Experimental Considerations

3.1 Photon Beam

We propose to use a linearly polarized beam of photons produced from the recently approved Coherent Bremsstrahlung Facility [23]. This technique of obtaining linearly polarized photons has successfully been employed at both SLAC [24] and Mainz [25]. Detailed discussions of the underlying theory of coherent bremsstrahlung can be found in references [26], [27], [28], and [29].

The spectrum of a photon beam produced coherently from a crystal radiator has several distinguishing characteristics compared with that of incoherent bremsstrahlung. The salient features of coherent bremsstrahlung are:

1. An energy spectrum with discrete peaks due to the varying contributions of different reciprocal lattice vectors
2. A strong linear polarization within each of the peaks
3. A polar angle distribution which is correlated with the energy of the photon
4. Tunable peak energies by crystal choice and orientation
5. The direction of the polarization can be quickly and smoothly changed by rotating the crystal radiator

We shall discuss each of these above points in turn.

For an electron of energy $E_\circ$ to radiate a photon of energy k requires that momentum $\vec{q}$ be transferred to a nucleus in the crystal lattice. The allowable range of momenta transfers are confined to the volume of a *pancakelike* region in momentum space, where the pancake conditions are given by

$$\delta \leq q_\ell \leq 2\delta \tag{9}$$
$$0 \leq q_\perp \leq 2x \tag{10}$$

where x is the fractional photon energy, $k/E_\circ$, and q_ℓ ($q_\perp$) is the longitudinal (perpendicular) momentum transfer. The minimum q_ℓ transferred can be expressed in terms of the fractional photon energy and the electron beam energy

$$\delta = q_\ell^{\min} = \frac{1}{2E_\circ}\frac{x}{1-x}. \tag{11}$$

We see then that a change in q_ℓ will produce a corresponding change in the coherent bremsstrahlung photon energy, $E_\gamma = xE_\circ$. We can locate this value of x by rotating the crystal with respect to the incident electron momentum. We will use the natural units ($\hbar = c = m_e = 1$) unless specifically marked otherwise. The influence of the crystal structure is given by the Laue condition

$$\vec{q} = \vec{g}. \tag{12}$$

Here $\vec{g}$ is the reciprocal lattice vector. Several reciprocal lattice vectors can contribute simultaneously if the orientation of the crystal with respect to the direction of the incident electron beam is not carefully selected. This leads to overlapping peaks which will smear out the direction of the polarization. For the following discussion we will follow the example of the Mainz group [25], and select the well isolated reciprocal lattice vector with the Miller indices of $(02\overline{2})$, which gives $|\vec{g}\,| = \frac{2\pi}{a}\sqrt{2^2+2^2}$, and where a is the length of the fundamental cell. For the case of diamond, $a = 925$ in dimensionless units. The corresponding momentum transfer to the lattice nucleus is then $|\vec{q}\,| = 9.85$ keV/c for $(02\overline{2})$. Selecting a specific q_ℓ in the range between δ and 2δ with respect to the electron momentum produces coherent-bremsstrahlung photons of the corresponding fractional energy x. Maximum linear polarization is found in the plane defined by the reciprocal lattice vector and the 3-momentum of the incident electron, i.e. $(\vec{g}, \vec{p}_\circ)$.

The angular distribution of the coherent and incoherent bremsstrahlung photons are very different. Whereas the polar angular distribution of the incoherent bremsstrahlung photons is *independent* of the photon energy

$$\frac{dN(\theta)}{d\theta} = \frac{\theta}{(1+\theta^2)^2}, \tag{13}$$

the emission angle of the coherent bremsstrahlung photons *decreases* with increasing photon energy ($x \leq x_d$)

$$\theta^2 = \frac{1-x}{x} 2E_\circ q_\ell - 1 = \frac{1-x}{x} \cdot \frac{x_d}{1-x_d} - 1. \tag{14}$$

Here x_d is the maximum fractional photon energy for a given setting of the crystal

$$x_d = \frac{2E_\circ q_\ell}{1+2E_\circ q_\ell}, \tag{15}$$

and the θs are given in units of characteristic angle, i.e.

$$\theta_{\rm char} = \frac{m_e c^2}{E_\circ}. \tag{16}$$

For example, for $E_\circ = 4.0$ GeV, $\theta_{\rm char} \simeq 1/8$ mrad.

We have developed a Monte Carlo which samples the probability density bremsstrahlung spectrum as a function of fractional energy x, and polar angle θ. The incoherent and coherent bremsstrahlung intensities as functions of x and θ are combined into one probability density function, which is based upon the derivations in ref. [29]. We have not yet incorporated the effects of multiple scattering, crystal mosaic spread, nor incident electron beam divergence. We assume that the crystal radiator is a thin wafer of diamond, and that only the reciprocal lattice vector $(02\bar{2})$ contributes to the coherent bremsstrahlung spectrum. For a given x ($x \leq x_d$) and θ, then, the ratio of the intensities of the uncollimated coherent and incoherent bremsstrahlung photons is quantified by the Debye temperature of diamond. Because of its relatively high Debye temperature, diamond is the preferred crystal for coherent bremsstrahlung production.

In Fig. 10 we overlay the incoherent and coherent polar angle distributions ($dN/d\theta$ vs θ). One sees a clearly delineated band in the scatter plot of the total photon counts (coherent + incoherent) as a function of characteristic angle and fractional photon energy (Fig. 11). We can then collimate the beam to reduce the incoherent background, which further serves to increase the degree of polarization. The maximum polar angle is limited by the opening angle of the collimator θ_{coll}, which gives a lower limit for coherent bremsstrahlung photon energy

$$x_{\min} = \frac{x_d}{1 + \theta_{\text{coll}}^2 (1 - x_d)}. \tag{17}$$

Therefore a spectral line in the energy region $x_{\min} \leq x \leq x_d$ remains for the collimated coherent bremsstrahlung photons. In Figs. 12a–d, we plot the total bremsstrahlung (coherent + incoherent) spectrum as a function of photon energy for four different collimator apertures overlayed upon the uncollimated spectra. And in Figs. 13a–d, the relative intensity for these four collimator settings, where we define

$$I_{\text{rel}} = \frac{I_{\text{coh}} + I_{\text{inc}}}{I_{\text{inc}}}, \tag{18}$$

and the intensity is proportional to $k\ dN/dk$. Finally, in Figs. 14a–d, we plot the degree of linear polarization as a function of x under four collimator settings for $E_\circ = 4.0$ GeV. If we collimate the photon beam to $\theta_{\text{coll}} = \theta_{\text{char}}/2$ (θ_{char}), we will obtain average polarizations of 70% (65%) for $1.98 \leq x \leq 2.2$ GeV ($1.85 \leq x \leq 2.20$ GeV).

Tightly collimating the beam to 0.125 mrad to provide a collimation of one half of a characteristic angle for Hall B should be reasonably straightforward. Using conventional techniques 25 years ago, SLAC was able to survey a collimator of diameter 2 mm at 91 m ($\theta_{\text{coll}} = 11\ \mu$rad) [30]. We are presently investigating the optimal crystal thickness. In order to keep the multiple scattering below one half of a characteristic angle, the thickness of the diamond radiator should not exceed 40 μm. The thickness of the crystal will determine the magnitude of the beam current required to provide 5×10^6 photons per second on the target after tight collimation and minimizing the tagger accidental rate. This subject is discussed in the next section.

3.2 Tagger Accidentals

We have performed a study employing the analysis code RATES.FOR [31] to determine the usable tagging rate with a coherent bremsstrahlung photon beam. We define an accidental as any charged particle that registers a hit in a TOF counter that occurs within 10 nsec of the $\gamma p \to \phi p$ event. We require that the beam be collimated to one half of a characteristic angle with the coherent peak set at a maximum of $E_\gamma = 2.20$ GeV for an incident electron beam energy of 4.0 GeV. We assume the LH_2 target to be of length 14 cm. We performed the study under varying the following conditions:

- The overall CLAS acceptance (from 60 to 80%) for any $\gamma + p$ event.
- The minimum 3-momentum required for a final-state proton or pion to pass through all three drift chamber regions and register a hit in a TOF counter. We assume that the reaction $\gamma p \rightarrow p\pi^\circ$ is twice as likely to occur as the $\gamma p \rightarrow n\pi^+$ channel. The final-state particles were distributed uniformly in c.m. phase space by the CERNLIB routine GENBOD [35]. We then determined the likelihood that the momentum of the particle exceeded the cutoff value. We expect the momentum cutoff values to vary as a function of angle in the CLAS. Below are our ranges in cutoff momenta of the final-state proton and pion.
    - $|\vec{p}_{\rm prot}| \geq 0.20$ GeV/c and $|\vec{p}_\pi| \geq 0.15$ GeV/c.
    - $|\vec{p}_{\rm prot}| \geq 0.20$ GeV/c and $|\vec{p}_\pi| \geq 0.20$ GeV/c.
    - $|\vec{p}_{\rm prot}| \geq 0.30$ GeV/c and $|\vec{p}_\pi| \geq 0.15$ GeV/c.
    - $|\vec{p}_{\rm prot}| \geq 0.30$ GeV/c and $|\vec{p}_\pi| \geq 0.20$ GeV/c.
- The number of triggers per second in the CLAS.

In Fig. 15 we plot the number of tagged photons striking the target after tight collimation as a function of the trigger rate for three overall CLAS acceptances of 60, 70, and 80%. We see that for an overall CLAS acceptance of 80% and trigger rate of 1 kHz, the number of tagged photons per second incident on the target is 4.23×10^6 Hz. This corresponds to a tagging rate of 2.04×10^7 Hz. In Figs. 16a–c we plot the percentage of accidentals per 10 nsec coincidence window versus CLAS acceptance as functions of both proton and pion momenta cutoff and trigger rate. We find for a trigger rate of 1 kHz, the percentage of accidentals to the total trigger rate is no worse than 33% with a CLAS acceptance of 80%

With our highly conservative estimate of setting the coincidence window to 10 nsec, we expect then that the ratio of reals to accidentals to be *at the very worst* 2:1 for $E_\circ = 4$ GeV for a photon flux on target of $4.2 \cdot 10^6$ Hz with a CLAS DAQ rate of 1 kHz. We are investigating the option of tightening the coincidence window to 4 nsec, which will signicantly reduce the accidental rate. Because the beam is continuous wave, we will be able to separate the primary from the accidental events by means of energy balance in the offline analysis. Finally, the accidentals will be from interactions distributed along the entire 14 cm length of the target. We will be able to remove almost all of these as they will be inconsistent with the reconstructed interaction position of the primary event.

3.3 Simulation

An acceptance study was performed by simulating events $\gamma p \rightarrow p\phi$ ($\phi \rightarrow K^+K^-$) and then passing these events through FASTMC_GEN [32]. The events were generated in the photon energy range $1.90 < E_\gamma < 2.20$ GeV ($2.11 < \sqrt{s} < 2.24$ GeV). For the purpose of the simulation, the average polarization was taken to be 65% (4 GeV electron beam). For a 6 GeV electron beam, the average polarization will be approximately 80%. The proton and ϕ meson were distributed in the cms frame according to the t dependence of the ϕ meson production cross section (Fig. 17). The decay kaons were distributed in the rest frame of the ϕ meson (helicity system) both uniformly in phase space and according to the SCHC distribution. The SCHC distribution was generated by sampling the probability density function binned in terms of $\cos\theta, \phi, \Phi$ weighted in accordance with the differential cross section described in equ. (1). All density matrix elements were set to zero except for $\rho^1_{1-1} = -Im\,\rho^2_{1-1} = 0.5$. We remark that the acceptance per bin in t, $\cos\theta$, ϕ, and Φ does not depend strongly upon the shape of the input photon distribution nor upon the shape of the decay distribution.

Background events for the reactions $\gamma p \rightarrow K^+\Lambda^*(1520)$ ($\Lambda^*(1520) \rightarrow pK^-$) and $\gamma p \rightarrow pK^+K^-$ (s-wave) were created using the routine GENBOD to generate the final-state particles pK^+K^- uniformly in phase space, where the photon energy E_γ was sampled uniformly in our energy bin. The $\Lambda^*(1520)$ events were weighted with a Breit-Wigner of width (, = 0.0156 GeV) and an exponential in four-momentum transfer ($\exp 6t$) [18]. The s-wave $K^+\ K^-$ pairs were generated over phase space and endowed with a conservative t dependence ($\exp 1.5t$) [22]. These background rates relative to ϕ meson signal will be discussed below. (cf. Sec. 3.5).

The generated events were then fed through FastMC_gen which renders a realistic representation the CLAS geometry with the attendant effects of multiple scattering and detector resolution for calculating our acceptances. The target parameters were consistent with that of the Saclay cryo-target (see Sec. 3.4). The magnetic field was set to the nominal field strength and half-nominal to find the optimal running conditions. The kaon decay probability used is an exponential form with a decay constant $c\tau = 3.709$ m. Events with K^+s that decayed in flight before hitting the TOF scintillators were not accepted. Fig. 18 displays the number of kaons arriving at each detector. For the energy range of this proposal, approximately half of the kaons decay in flight to the scintillators.

The momentum range of the detected kaon (proton) is shown in Fig. 19-a(b), with the relative accuracy of the momentum measurement as depicted in Fig. 19-c(d). The CLAS detector can separate kaons from pions cleanly in this momentum range via the method of time of flight [33]. Detection of the final-state proton and K^+ meson combined with a measurement of the energy of the tagged photon overdetermine the kinematics and allow for a missing 4-momentum reconstruction of the K^- meson. From the 4-momenta of these final-state kaons, we can then determine the invariant mass of the ϕ meson . If we naively use the missing 4-momentum of the K^-, our measurement uncertainty in the ϕ mass (3.4 MeV) is dominated by the uncertainty in the photon energy as measured by the tagger system. By constraining the invariant mass of the K^- 4-momentum to the known kaon mass, we effectively remove this contribution; reducing the ϕ mass uncertainty to 1.2 MeV. This measurement uncertainty is sufficiently small that the shape (see Fig. 23) is dominated by the natural width of the ϕ.

The acceptance ($N_{\text{detected}}/N_{\text{generated}}$) as a function of t is shown in Fig. 20 and Table 3. The acceptance increases as $|t|$ increases. This is a result of the kinematics. Since the ϕ mesons are produced near threshold, the reaction products are confined to a narrow, forward cone in the laboratory and most events are lost down the beam pipe. As t increases, the transverse momentum of the reaction products increases – giving a higher detection probability in the CLAS. Note that the acceptance decreases only about 10-15% when the phase space containing the $\Lambda^*(1520)$ is cut out. Two dimensional histograms of acceptance as a function of ϕ_{K^+} vs. $\cos\theta_{K^+}$ support this explanation and are shown in Figs. 21 and 22.

All t bins have complete coverage in $\cos\theta_{K^+}$ with coverage in ϕ_{K^+} increasing as t increases. This acceptance is complete enough to allow the extraction of the density matrix elements (see Sec. 3.6).

3.4 Count Rate Estimate

The Monte Carlo simulation provided the acceptance for the count rate estimate described here. The tagger accidentals study results in the factor of 0.7. The formula used to calculate the count rate is

$$N(\text{events/sec}) = 0.7 N_{\text{tgt}} \frac{d\sigma}{dt} \Delta t \, \varepsilon (\text{BR}) \Phi \tag{19}$$

where

$$N_{\text{tgt}} = \frac{\rho_{\text{LH}_2} \ell N_A (N_{protons}/LH_2)}{A_{\text{LH}_2}} \tag{20}$$

and

$$\frac{d\sigma}{dt} = \left.\frac{d\sigma}{dt}\right|_{t=0} \exp\left(6t + 1.4t^2\right) \tag{21}$$

The parameters of the equation are defined as:

Δt:	bin width
ε:	t bin acceptance
BR = 0.491:	branching ratio of $\phi \to K^+K^-$
$\mathbf{\Phi}$:	the photon flux ($4.5 \cdot 10^6$ γ/sec)
$\rho_{\text{LH2}} = 0.071$ g/cm^2:	density of liquid hydrogen
$\ell = 14$ cm:	length of the Saclay cryo-target
N$_A$:	Avagadro's number
(N$_{\text{protons}}$/LH$_2$):	2
A$_{\text{LH}_2}$ = 2.016	atomic weight of liquid hydrogen
$\left.\frac{d\sigma}{dt}\right\|_{t=0} = 1.0 \frac{\mu\text{b}}{(\text{GeV/c})^2}$	forward differential cross section for $E_\gamma = 2$ GeV [17]

The count rates and total counts for a running period of 500 hours are contained in Table 3. The expression for the differential cross section is from Ref. [3]. Since the fundamental processes are predicted to have different t dependences, the data will be binned in terms of the four-momentum transfer in order to measure the t evolution of the spin density matrix elements. For example, the mid- and high-t bins are expected to contain less diffractive components than the low-t bins. In order to obtain the desired sensitivity in each t bin of 10% on the extracted value of the density matrix elements, about 1000 counts/bin are needed in the mid-t region. Due to the lower acceptance at low-t more counts are needed for the fit, which is compensated by the higher count rate in the forward region. The width of the largest $|-t|$ bins has been adjusted to keep the statistics constant with the mid-t bins.

t (GeV/c)^2	Δt	$d\sigma/dt$ μbarns/GeV^2	ε	counts	ε $\Lambda(1520)$ cut	counts $\Lambda(1520)$ cut
-0.25	0.1	0.633	0.102	4105	0.089	3582
-0.35	0.1	0.378	0.130	3123	0.110	2643
-0.45	0.1	0.232	0.144	2124	0.126	1858
-0.55	0.1	0.146	0.163	1517	0.140	1303
-0.70	0.2	0.077	0.172	1693	0.154	1516
-1.00	0.4	0.026	0.147	977	0.127	844

Table 3: Count rate estimate for 500 hours of running with 30% accidentals.

3.5 Background Rates

The primary source of background contamination for this experiment are due to pions, kaons from the reaction $\gamma p \to K^+\Lambda^*$ ($\Lambda^* \to K^-p$), and s-wave K^+K^- pairs. It has been shown that kinematical cuts are effective in removing the pion background [22]. We will therefore only address the contamination from the Λ^*, and s-wave K^+K^- mechanisms.

For the proposed energy range of $2.11 \leq \sqrt{s} \leq 2.24$ GeV, the decay product from $\Lambda^*(1520)$ will contribute to the K^+K^- invariant mass spectrum. The total cross section for $\gamma p \to K^+\Lambda^*(1520)$ at $E_\gamma = 2$ GeV is approximately 0.8 μb [18]. This background to the event total has been scaled to the K^+K^- cross section (0.160 μb [17]) from ϕ photoproduction at $E_\gamma = 2.0$ GeV, which is shown in Figs. 24 and 26.

The acceptance and count rate has been calculated with and without a cut on the $\Lambda^*(1520)$ mass (see Table 3). Eliminating the $\Lambda^*(1520)$ from the data pool reduces the overall acceptance by only 10–15%. Because of the large acceptance CLAS, full angular coverage of the decay kaons from ϕ decay is still achieved allowing for the extraction of the spin density matrix elements. Since the angular distribution of the final-state kaon arising from the $\Lambda^*(1520)$ decay is well known, including this hyperon in our density matrix fitting procedure is possible.

Although the $\Lambda^*(1520)$ is treated as a background in the rest of this proposal, one man's background is another man's physics. The estimated cross section would lead to an even larger sample of $\Lambda^*(1520)$ than ϕ in the proposed data set. We should be able to extract density matrix elements for this reaction of a similar quality to that of the ϕ. This will provide a $Q^2 = 0$ measurement, which will complement the approved electroproduction experiment (E89-043) [19].

S-wave kaons are also a source of contamination in the K^+K^- invariant mass spectrum for the proposed measurement [17], [20]. An estimate of 1.5 μb for the total resonant plus nonresonant s-wave K^+K^- photoproduction cross section (see Fig. 25) would correspond to a 25% contamination of the K^+K^- invariant mass spectrum in the range of the ϕ mass (see Fig. 24).

The resonant s-wave K^+K^- pairs will provide information on the reaction $\gamma p \to a_0(980)p \to K^+K^-p$. It will be possible to extract a signal from the reaction $\gamma p \to a_0(980)p \to K^+K^-p$ [17], [20]. When taking into account the a_0 contribution both resonances, a_0 and ϕ, are parametrized via Breit-Wigner distributions convoluted with Gaussian functions. The ϕ contribution is then extracted by fitting all three mass shapes: a_0, ϕ, and phase-space background.

The projection of Fig. 24 onto the $m_{K^+K^-}$ axis is shown in Fig. 26. The shaded histogram is the result of removing the K^+K^- pairs associated with a $\Lambda^*(1520)$ via a mass cut on m_{pK^-}. It is shown in Sec. 3.6 that the density matrix elements describing ϕ production can be reliably extracted from the shaded histogram which contains the ϕ production data with an s-wave K^+K^- background.

3.6 Density Matrix Element Extraction

The data are binned in a 3-dimensional histogram $W(\cos\theta, \phi, \Phi)$ for events in the ϕ peak ($1.015 < M_{K^+K^-} < 1.025$). The reflection of the $\Lambda^*(1520)$ was removed from the data with a mass cut on m_{pK^-}. An estimate of the remaining background was obtained by analyzing counts in bins on both sides of the resonance peak as in Ref. [17]. (see Fig. 25) Events from the ϕ sidebands ($0.995 < M_{K^+K^-} < 1.005$ and $1.035 < M_{K^+K^-} < 1.045$) are also binned in the three variables, $\cos\theta$, ϕ, and Φ. These are scaled to the number of events under the ϕ window, to estimate the angular distribution of the background. Alternatively, if the distributions are not consistent in the low and high sidebands, for this purpose phase-space distributed MC data of the reaction $\gamma p \to K^+K^-p$ can be analyzed to get a polynomial parametrization of the K^+K^- mass distribution near the ϕ mass (1.019 GeV) [34].

A maximum-likelihood fit was performed on the data using MINUIT [35] with equ. 1 to extract the density matrix elements. The convergence of the fitting procedure was studied as a function of bin size, parameter starting values, and step sizes. The weight function (equ. 1 is integrated over the bins in $(\cos\theta, \phi, \Phi)$ in order to account for variations in the function over the bin interval.

Fig. 27 shows the results of the determination of ρ^1_{1-1} and $Im\ \rho^2_{1-1}$ from the SCHC simulated data. The error bars include statistics, and 10% error on the polarization and a 10% contribution from systematic errors in the fit. The circles on the figure are the data from the Ballam group [15] (see Table 4). The squares are the results of the fit to a background free spectrum and the triangle are the results of the fit to the data plus background. The solid lines on the figure indicate the input values to the simulation. The figure shows the improvement we expect over the old data. The results indicate that we have the ability to extract the density matrix elements in each t bin with a sensitivity better than has been measured before. This sensitivity, combined with the range in t, will allow us to differentiate between various predictions for the threshold behavior of ϕ photoproduction.

3.7 Beam Time Request

We request 100 hours of 4 GeV electron beam time and 400 hours of 6 GeV electron beam time with the approved coherent bremsstrahlung photon facility installed. The CLAS magnetic field will be set to half field and the Saclay cryo-target installed in its normal position. The photon tagger will be set to accept electrons from unpolarized photons above and below the coherent peak allowing unpolarized data taking simultaneously with polarized data. The 4 GeV data will serve as a tune-up run and allow an initial look at ϕ production and the associated backgrounds. Because of significant overlap of the experimental setup of E94-109 (photoproduction of ρ mesons from the proton with linearly polarized photons), we have agreed to work closely with that collaboration, sharing resources and manpower. The experiment proposed here uses the identical apparatus other than the need to reorient the diamond crystal to achieve higher photon beam energies. We therefore seek to run as a continuation of the $\gamma 8$ period to minimize experimental overhead.

Data for final analysis will be taken with the 6 GeV electron beam; it provides greater photon polarization thus reducing systematic errors. At this energy setting, the possibility exists to share some beam time with E94-109; our request takes this overlap into account. We further request an additional 400 hours with the crystal oriented to maximize the photon polarization at the energies required for the present experiment. To optimally use the resources of the lab and the collaborators of this experiment and E94-109, we seek to run as a continuation of the $\gamma 8$ run period.

4 Summary

A high-precision measurement of the nine spin density matrix elements of the reaction $\vec{\gamma} p \rightarrow \phi p$ will significantly add to our knowledge of the contributing processes beyond diffraction. The measurement of the angular distribution of the decay kaons as a function of t will quantify the contributions of the natural and unnatural parity exchange to the production cross section. A marked departure from zero of seven of the nine measureable density matrix elements will signal new production mechanisms. This experiment will provide results complementary to the two approved CLAS experiments, E93-022 and E93-031.

References

[1] N. Isgur, JLAB-THY-96-14.

[2] M.A. Pichowsky, Ph.D. Thesis, University of Pittsburgh (1996).

[3] T.H. Bauer, R.D. Spital, D.R. Yennie, and F.M. Pipkin, Rev. Mod. Phys. **50**, 261 (1978).

[4] T.J. Ketel, Ph.D. Perspectives in the Structure of Hadronic Systems, Plenum Press, New York (1994).

[5] J. Gasser, H. Leutwyler, and M.E. Sainio, Phys. Lett. **B253**, 163 (1991).

[6] E.M. Henley *et al.*, Phys. Lett. **B281**, 178 (1992).

[7] A.I. Titov, Y. Oh, and S.N. Yang, Chin. Jour. Phys. **32**, 1351 (1994).

[8] R. Williams, *private communication.*

[9] K. Schilling, P. Seyboth, and G. Wolf, Nucl. Phys. **B15**, 397 (1970).

[10] F. Cooper, Phys. Rev. **170**, 1602 (1968).

[11] R.L. Thews, Phys. Rev. **175**, 1749 (1968).

[12] P.L. Cole *et al.*, CEBAF E94-109.

[13] C.G. Fasano *et al.*, Phys. Rev. **C46**, 2430 (1992).

[14] H.J. Halpern *et al.*, Phys. Rev. Lett. **29**, 1425 (1972).

[15] J. Ballam *et al.*, Phys. Rev. **D7**, 3150 (1973).

[16] G. McClellan *et al.*, Phys. Rev. Lett. **46**, 1597 (1971).

[17] D.P. Barber *et al.*, Z. Phys. **C12**, 1 (1982).

[18] D.P. Barber *et al.*, Z. Phys. **C7**, 17 (1980).

[19] L. Dennis *et al.*, CEBAF E89-043.

[20] D.C. Fries *et al.*, Nuc. Phys. **B143**, 408 (1978).

[21] E.S. Smith *et al.*, CEBAF E93-022.

[22] C. Marchand *et al.*, CEBAF E93-031.

[23] K.S. Dhuga, *private communication.*

[24] W. Kaune *et al.*, Phys. Rev. **D11**, 478 (1975).

[25] D. Lohman *et al.*, Nucl. Instr. Meth. **A343**, 494 (1994); J. Peise, M.S. Thesis, Universität Mainz (1989); D. Lohman, M.S. Thesis, Universität Mainz (1992); F. Rambo, M.S. Thesis, Universität Göttingen (1995); A. Schmidt, M.S. Thesis, Universität Mainz (1995).

[26] F.H. Dyson and H. Überall, Phys. Rev. **99**, 604 (1955);
H. Überall, Phys. Rev. **103**, 1055 (1956).

[27] H. Überall, Phys. Rev. **107**, 223 (1957); see also Z. Naturforsch. **17a**, 332 (1962).

[28] G. Diambrini-Palazzi, Revs. Modern Phys. **40**, 611 (1968).

[29] U. Timm, Fortschr. Phys. **17**, 765 (1969).

[30] C. Sinclair, *private communication.*

[31] D.I. Sober, *private communication.*

[32] P.L. Cole, "A Generalized FastMC for the CLAS," CLAS-NOTE 93-006;
E.S Smith, "Fast Monte Carlo for the CLAS Detector," CLAS-NOTE 90-003.

[33] "CLAS Conceptual Design Report" (1990).

[34] F.J. Klein, BONN-IR-96-08, (1996).

[35] CERN program library - CERNLIB-94A.

List of Tables

List of Figures

	$2.8 < E_\gamma < 4.7$ (GeV)	$E_\gamma = 9.3$ (GeV)
ρ^0_{00}	-0.04 ± 0.06	0.00 ± 0.07
$Re\rho^0_{10}$	-0.00 ± 0.06	-0.01 ± 0.06
ρ^0_{1-1}	-0.04 ± 0.10	-0.14 ± 0.09
ρ^1_{00}	-0.13 ± 0.09	0.08 ± 0.12
ρ^1_{11}	-0.06 ± 0.11	-0.18 ± 0.13
$Re\rho^1_{10}$	0.00 ± 0.09	-0.20 ± 0.11
ρ^1_{1-1}	0.18 ± 0.13	0.44 ± 0.15
$Im\rho^2_{10}$	-0.02 ± 0.10	-0.14 ± 0.09
$Im\rho^2_{1-1}$	-0.51 ± 0.16	-0.73 ± 0.17

Table 4: Ballam group density matrix elements for ϕ photoproduction. [15]

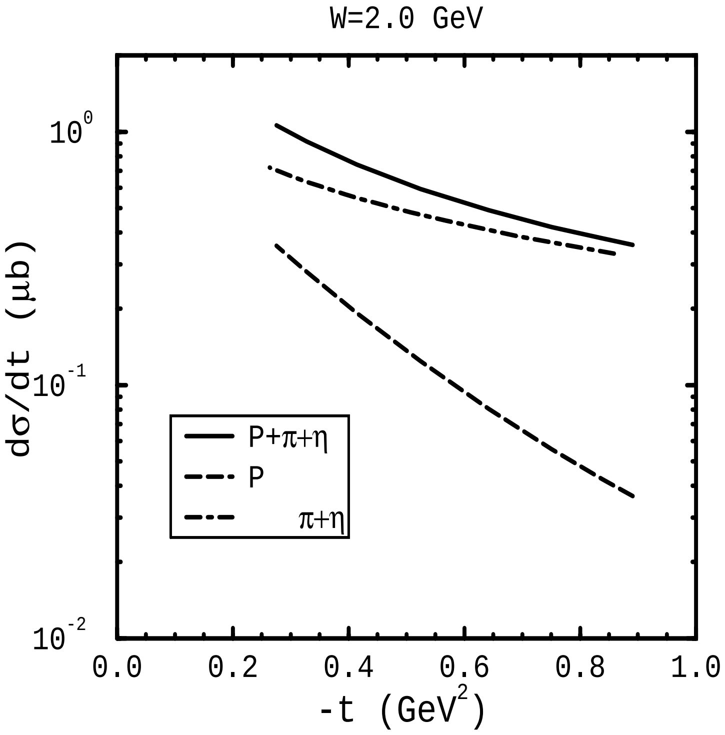

Figure 1: Differential cross section prediction from pomeron + meson model [2].

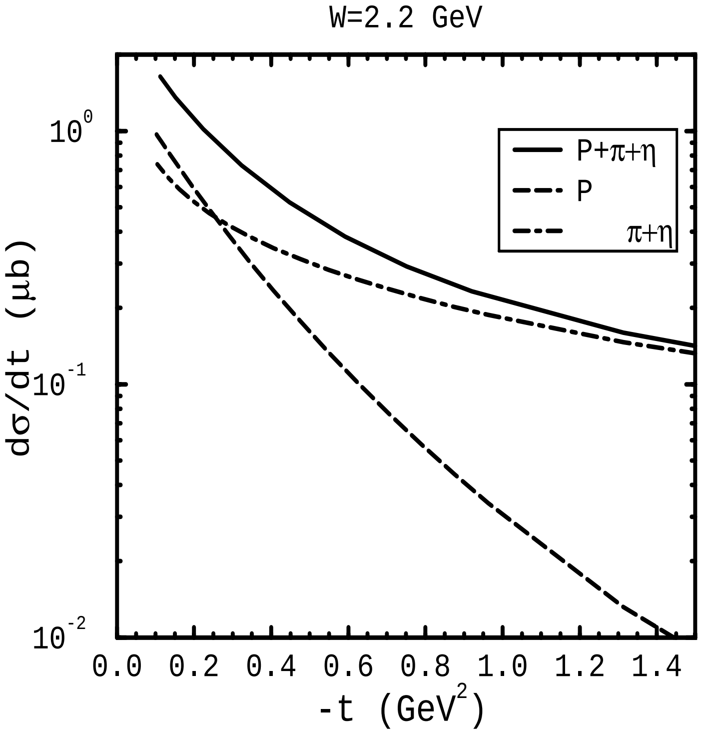

Figure 2: Differential cross section prediction from pomeron + meson model [2]. Please note the change in scale from Fig. 1.

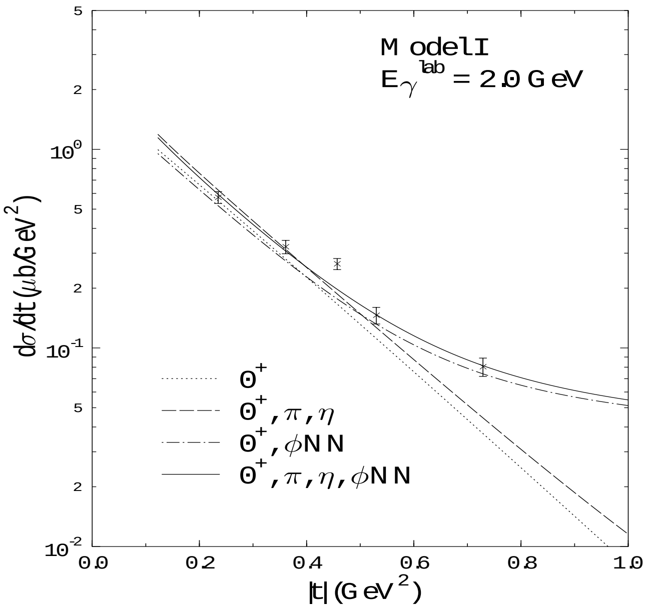

Figure 3: Differential cross section calculation including pomeron exchange (0^+) + meson exchange (π, η) + OZI evading processes (ϕNN) [8].

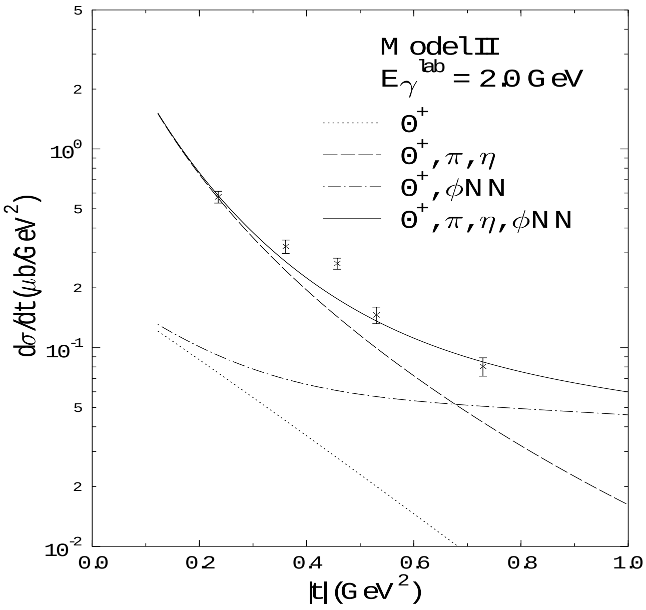

Figure 4: Differential cross section calculation including pomeron exchange (0^+) + meson exchange (π, η) + OZI evading processes (ϕNN) [8].

Figure 5: Helicity system angle definitions.

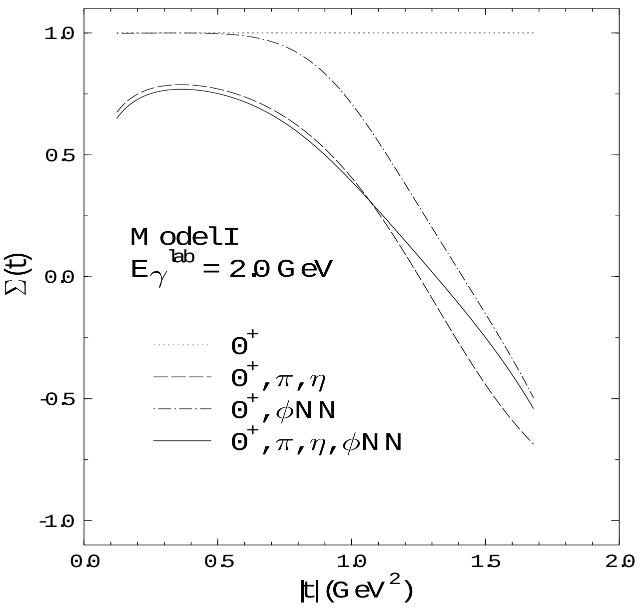

Figure 6: Asymmetry parameter calculation including pomeron exchange (0^+) + meson exchange (π, η) + OZI evading processes (ϕNN) [8].

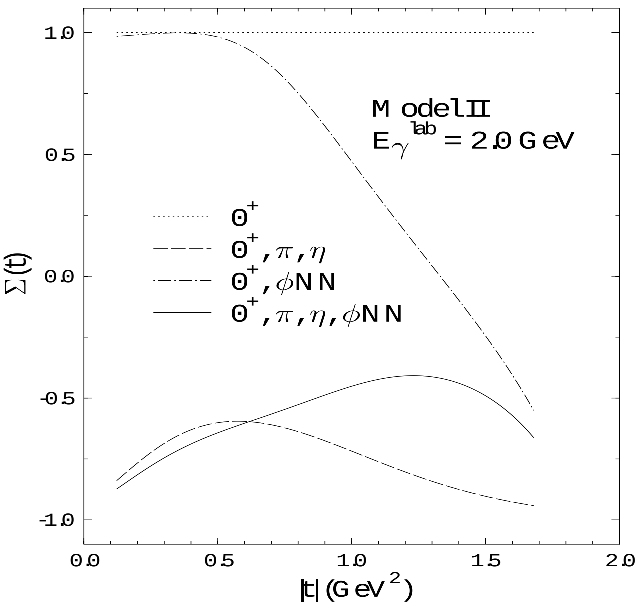

Figure 7: Asymmetry parameter calculation including pomeron exchange (0^+) + meson exchange (π, η) + OZI evading processes (ϕNN) [8].

Figure 8: Kaon decay distributions from Ballam [15].

Figure 9: Unpolarized differential cross section data of Barber et al. [17]

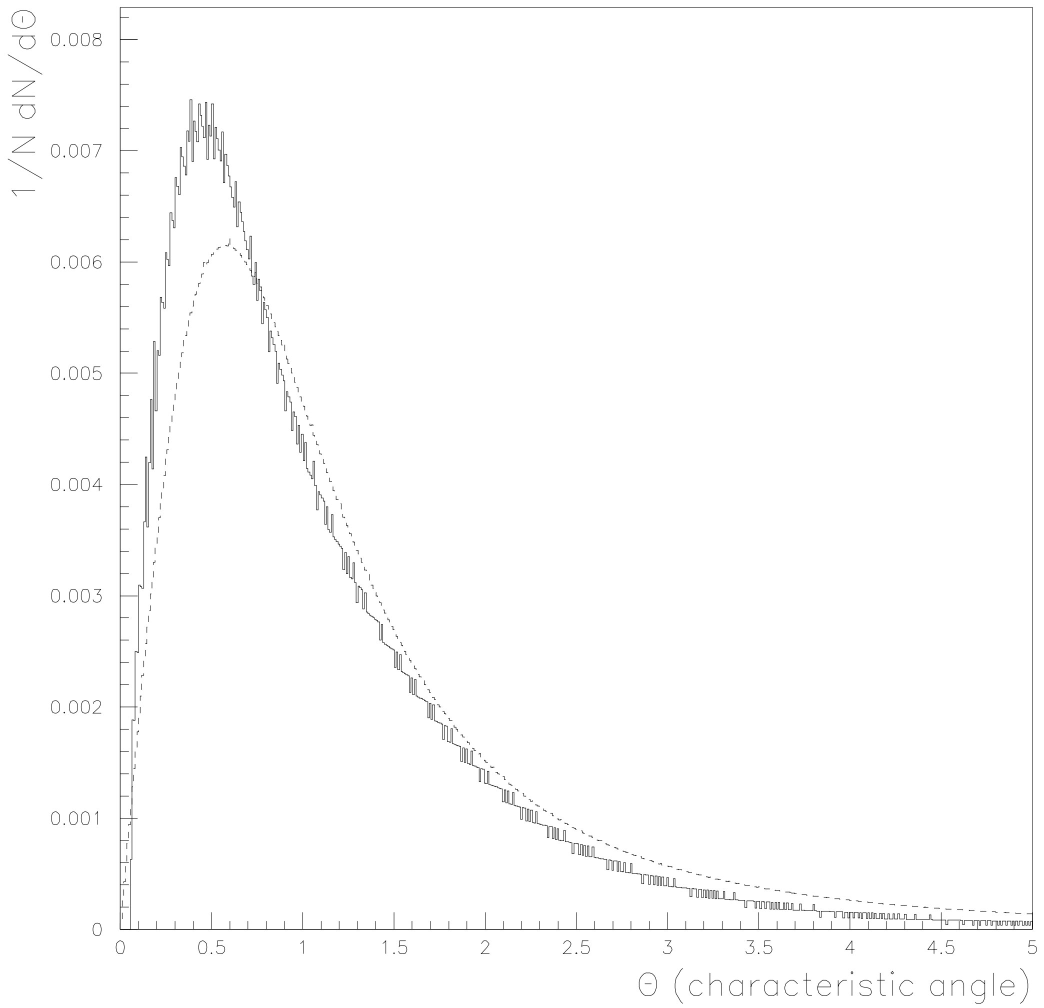

Figure 10: Overlay of the normalized polar angle distributions for coherent (solid) and incoherent (dashed).

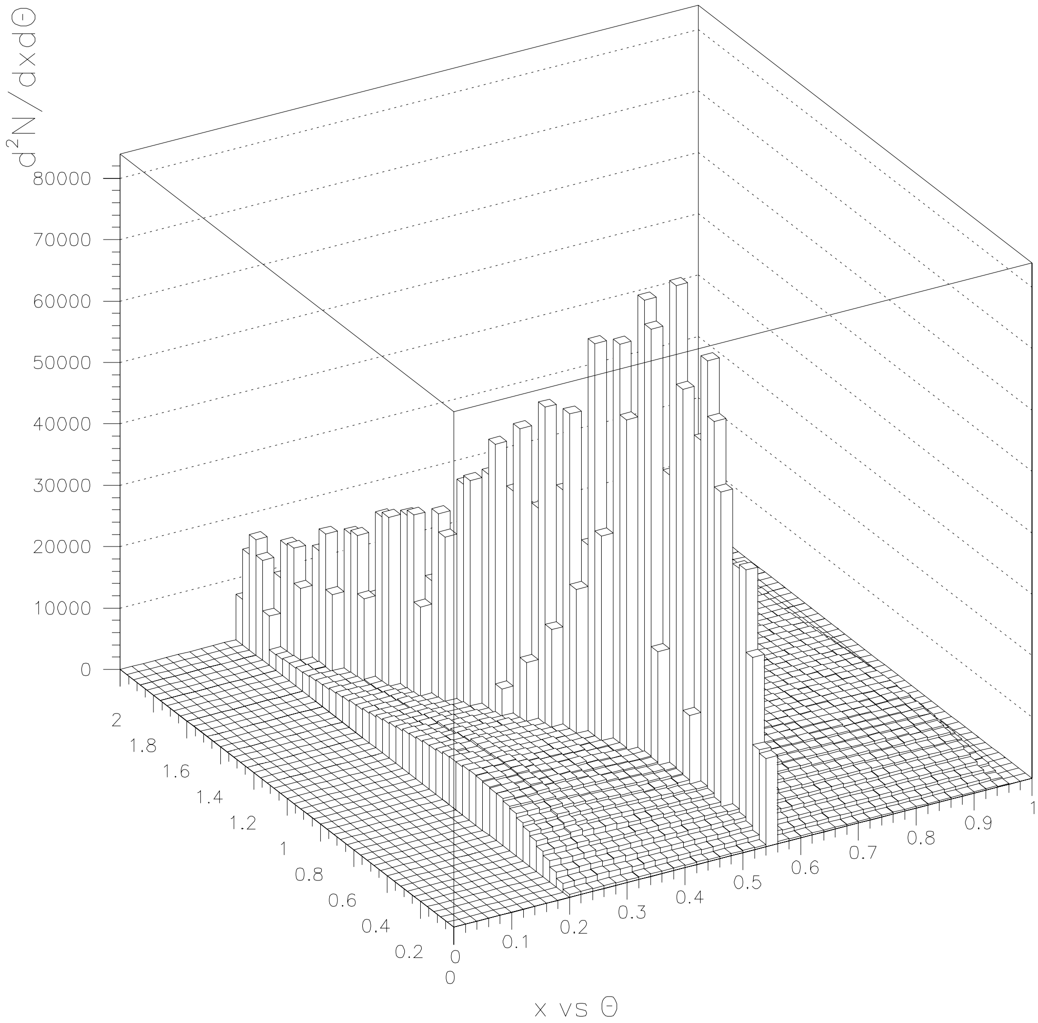

Figure 11: Number of photons per bin in fractional photon energy $x = k/E_\circ$ and polar angle in units of characteristic angle $[m_e c^2/E_\circ]$ for the sum of coherent and incoherent bremsstrahlung, here $x_{\max} = 0.55$.

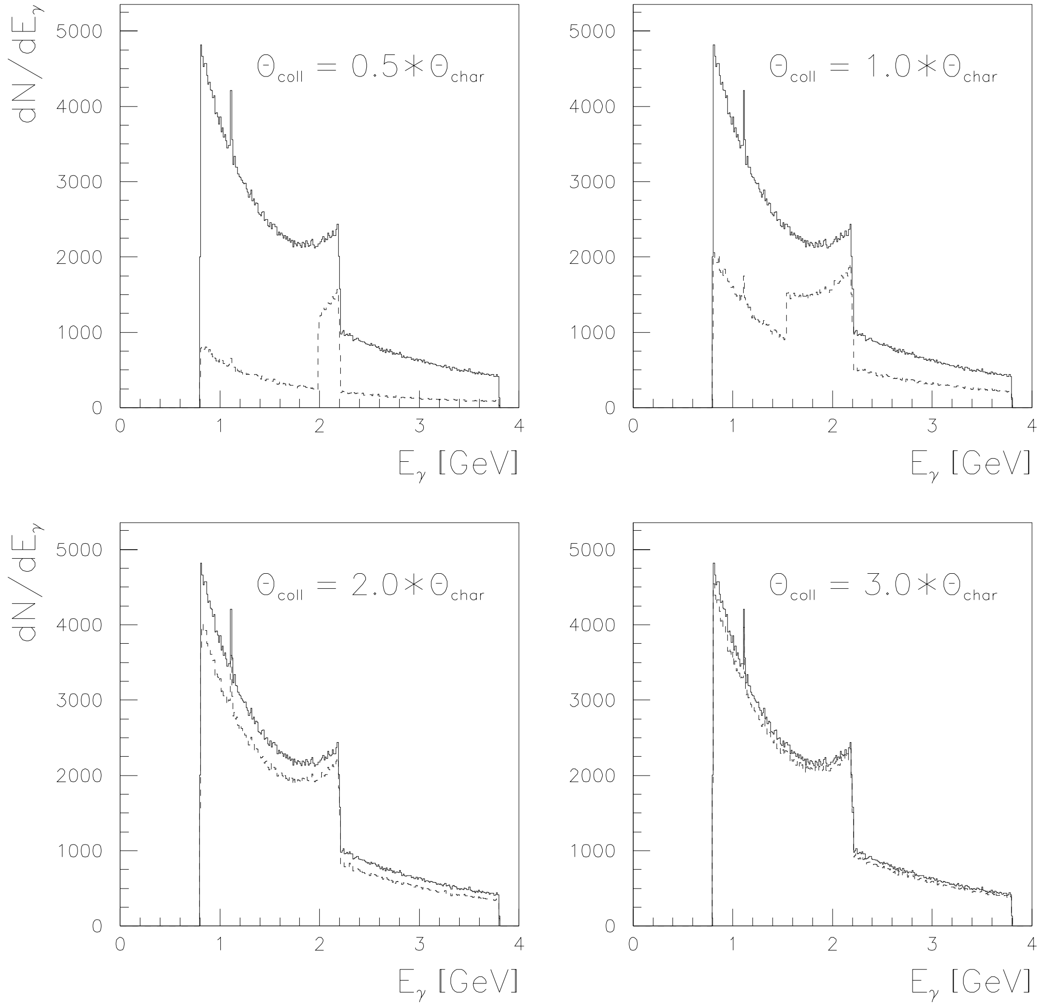

Figure 12: Superimposed coherent (dashed) and incoherent (solid) dN/dE_γ vs E_γ bremsstrahlung distributions under various collimator opening angles.

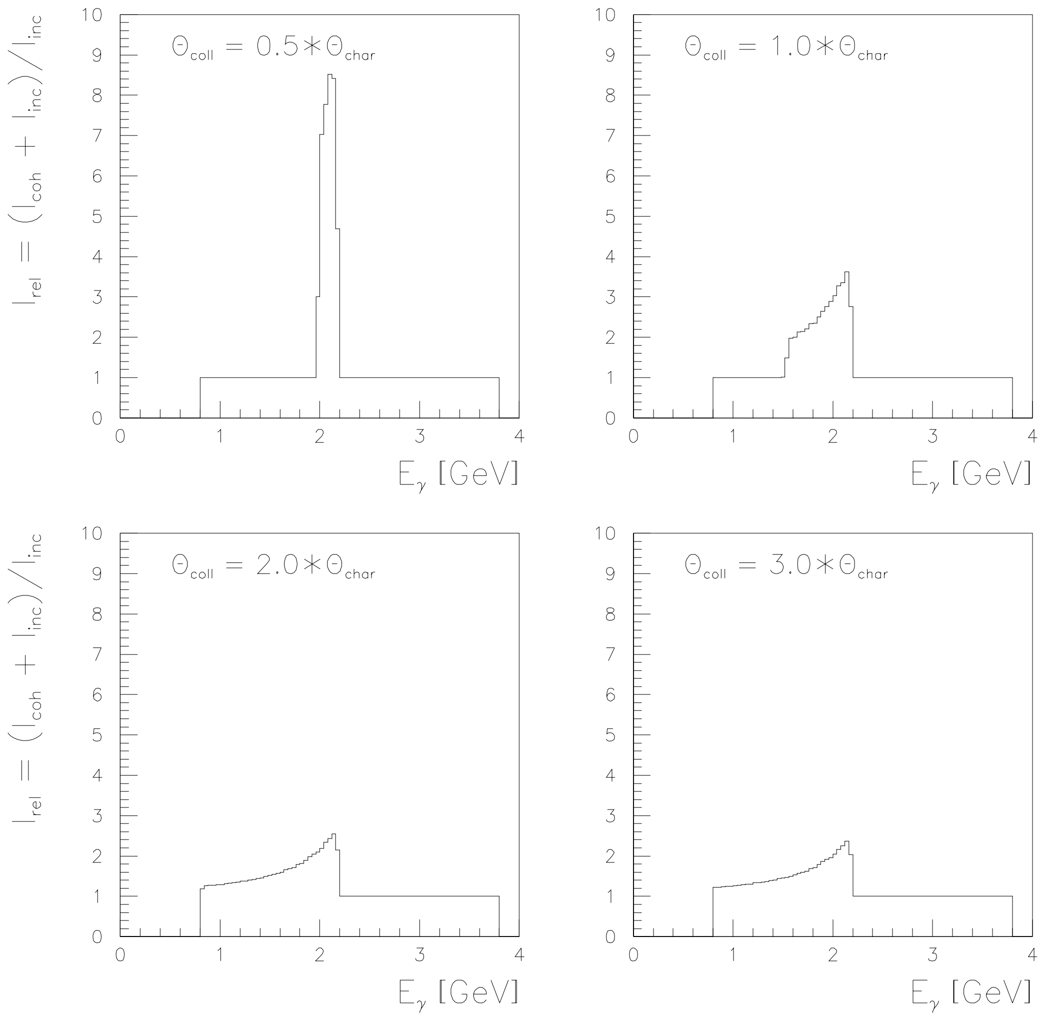

Figure 13: The relative intensity as a function of photon energy under various collimator opening angles. $I_{\rm rel} = I_{\rm tot}/I_{\rm inc}$ and $I \propto E_\gamma \cdot dN/dE_\gamma$.

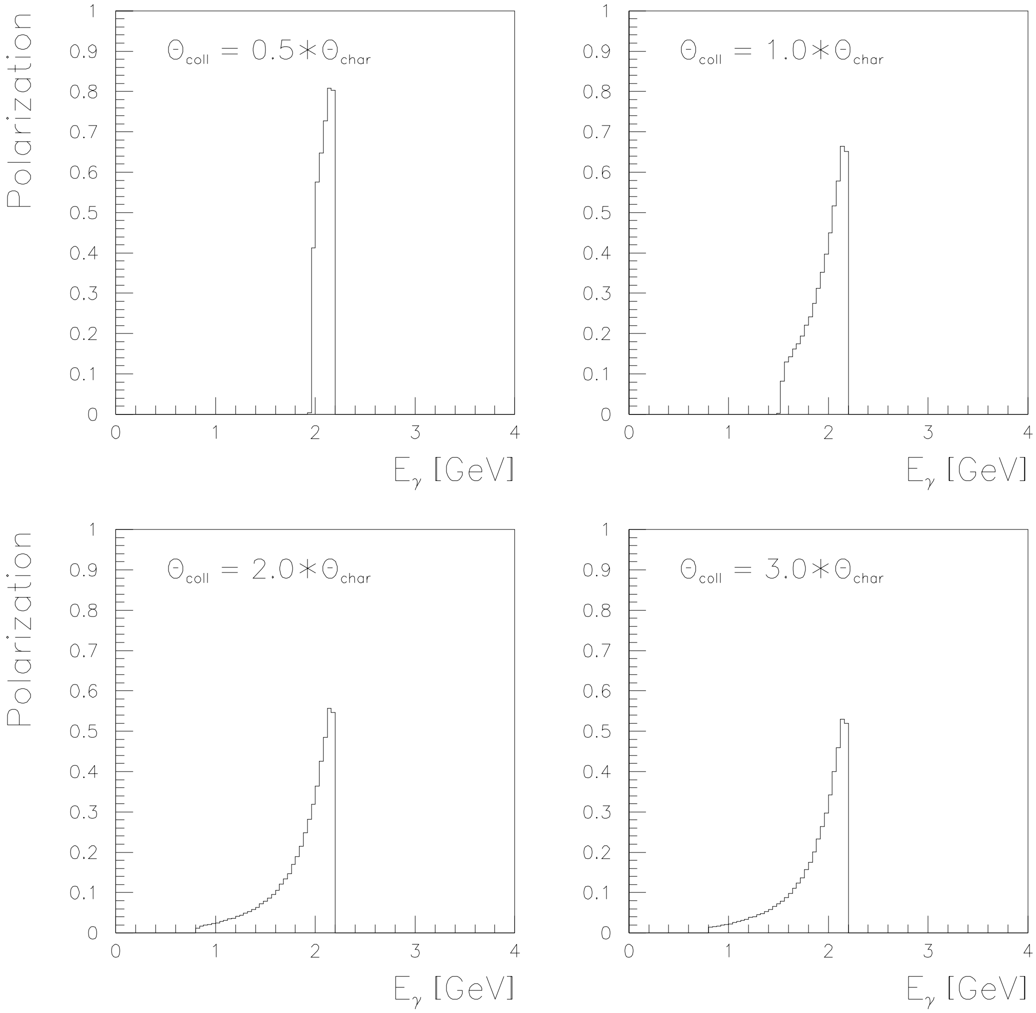

Figure 14: Polarization of coherent bremsstrahlung spectral line as a function of photon energy for various collimator opening angles.

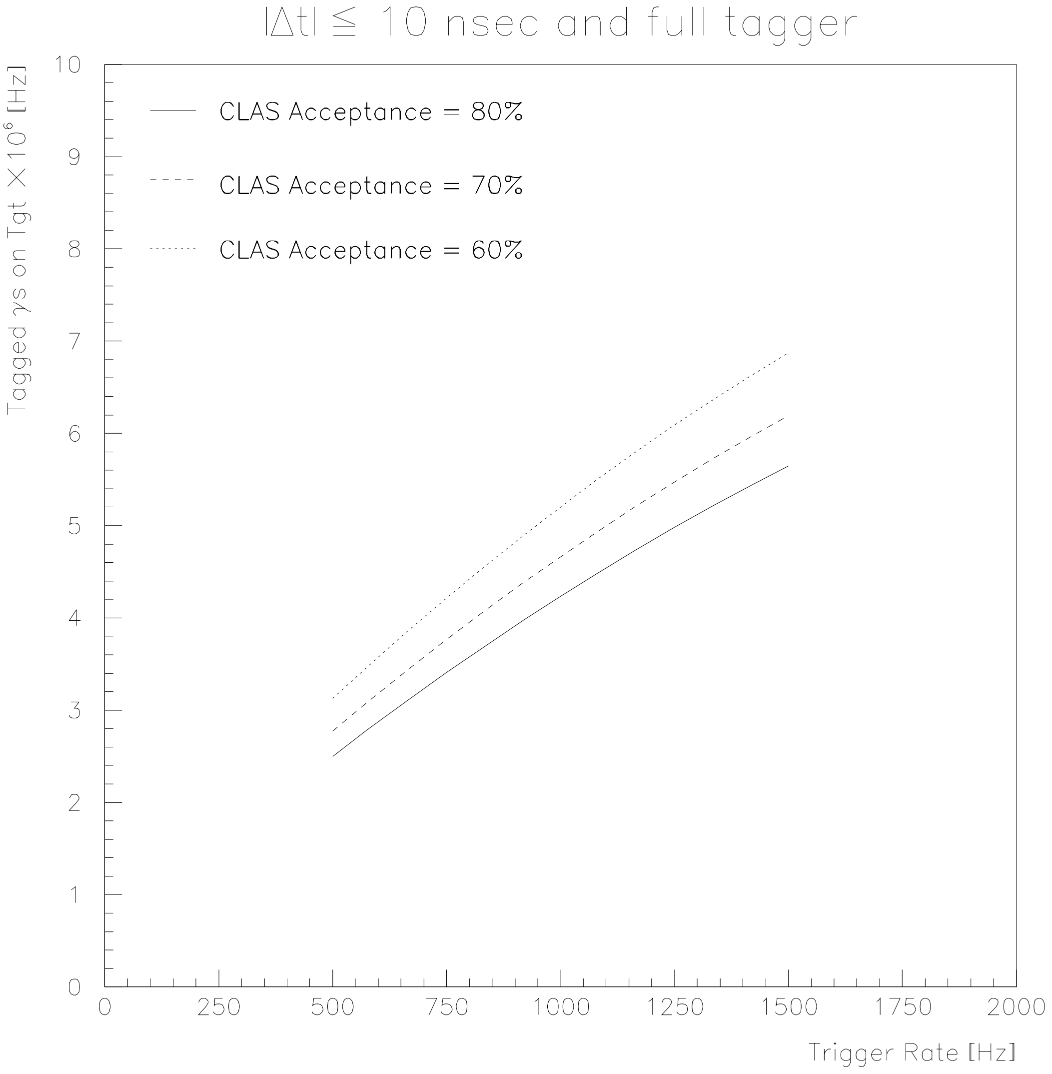

Figure 15: Collimated photons vs trigger rate as functions of the overall CLAS acceptance. We have set the collimation aperture to one half of a characteristic angle.

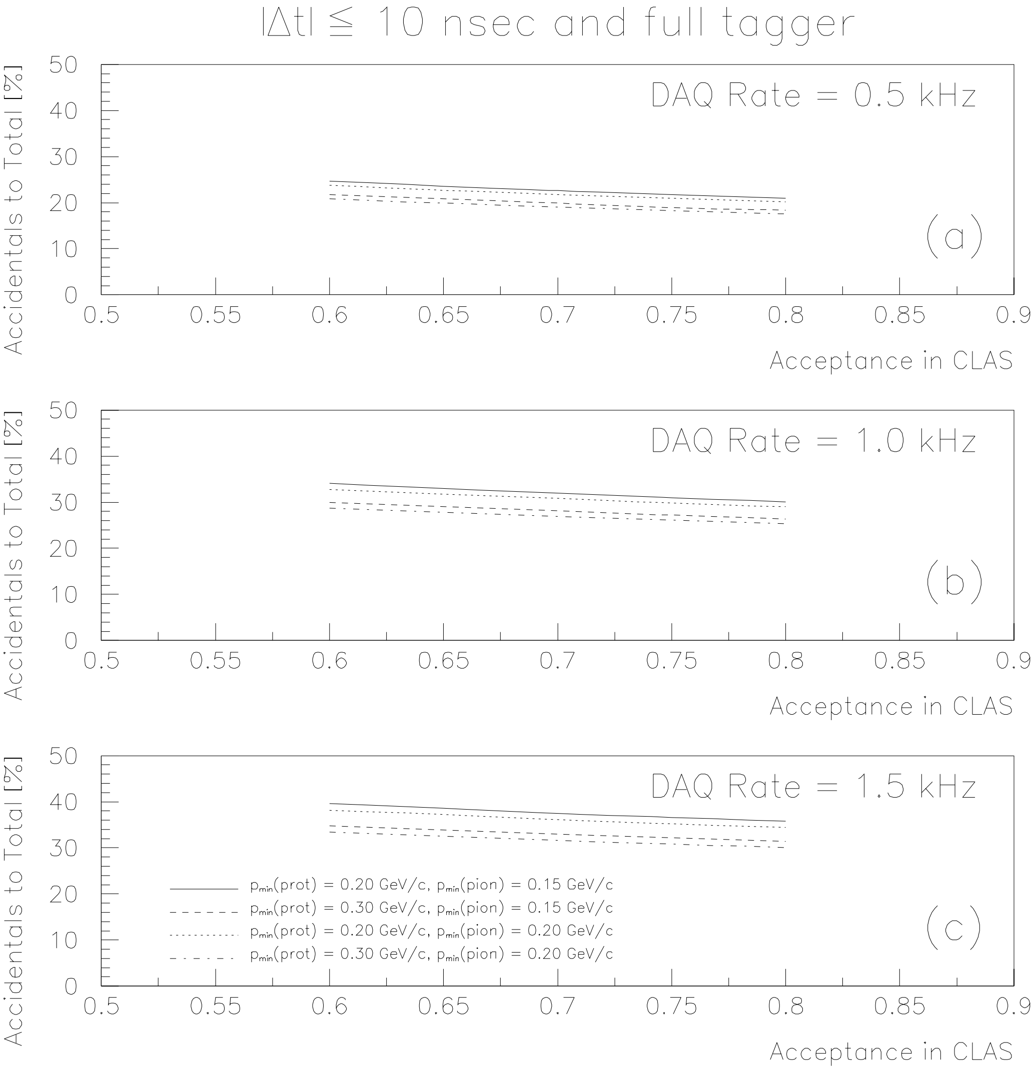

Figure 16: Percentage of accidentals vs the overall CLAS acceptance as functions the cutoff momenta of final-state protons and pions for trigger rates: (a) 500 Hz, (b) 1000 Hz, and (c) 1500 Hz.

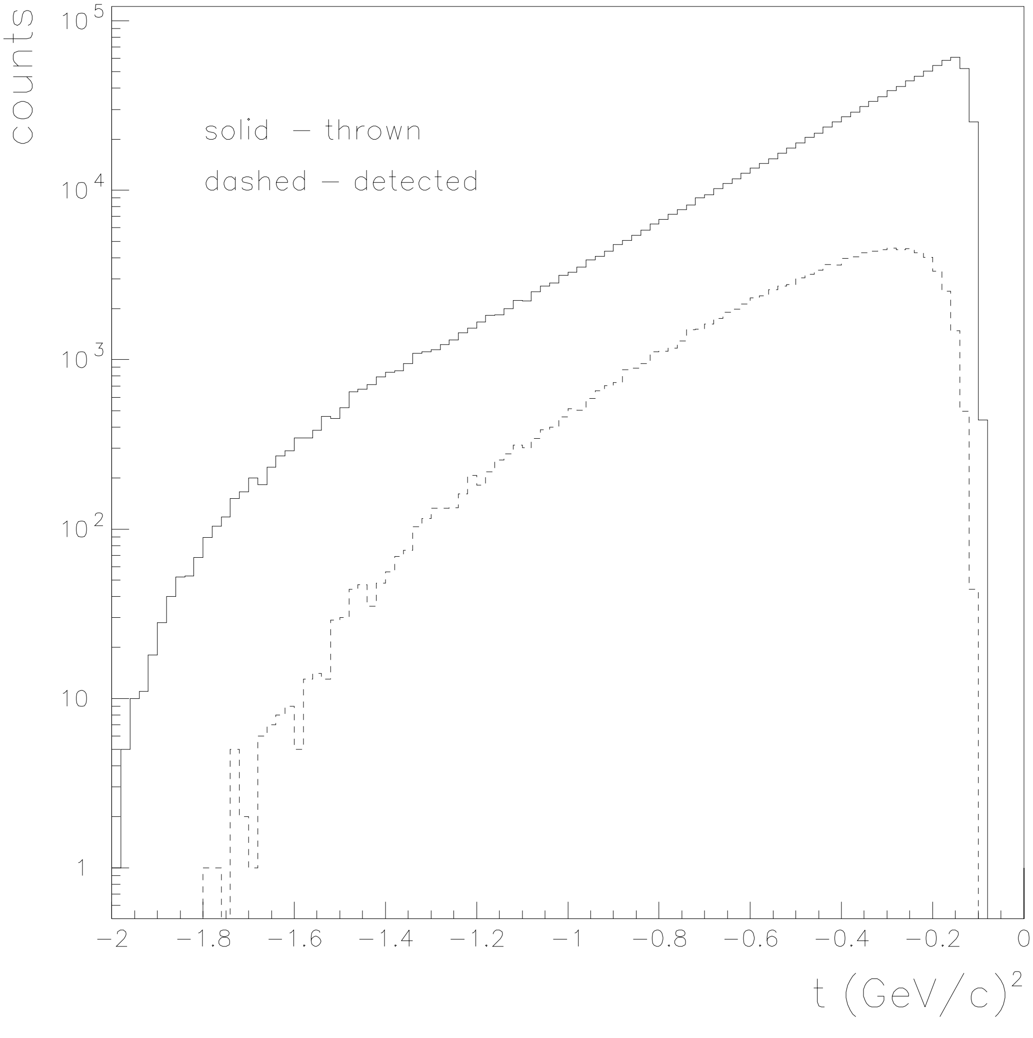

Figure 17: Four-momentum transfer squared (t) distribution; (solid line) sampled from the event generator and (dashed line) reconstructed after processing through FastMC_gen.

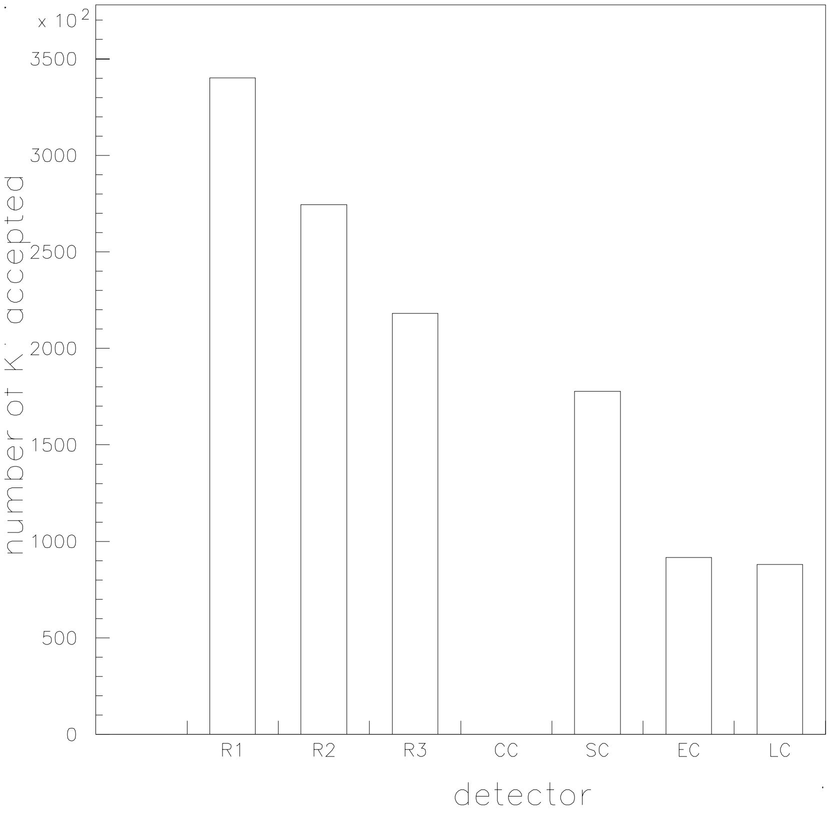

Figure 18: Number of K^+ mesons reaching each detector component. Accepted events must register a hit in a TOF counter (SC).

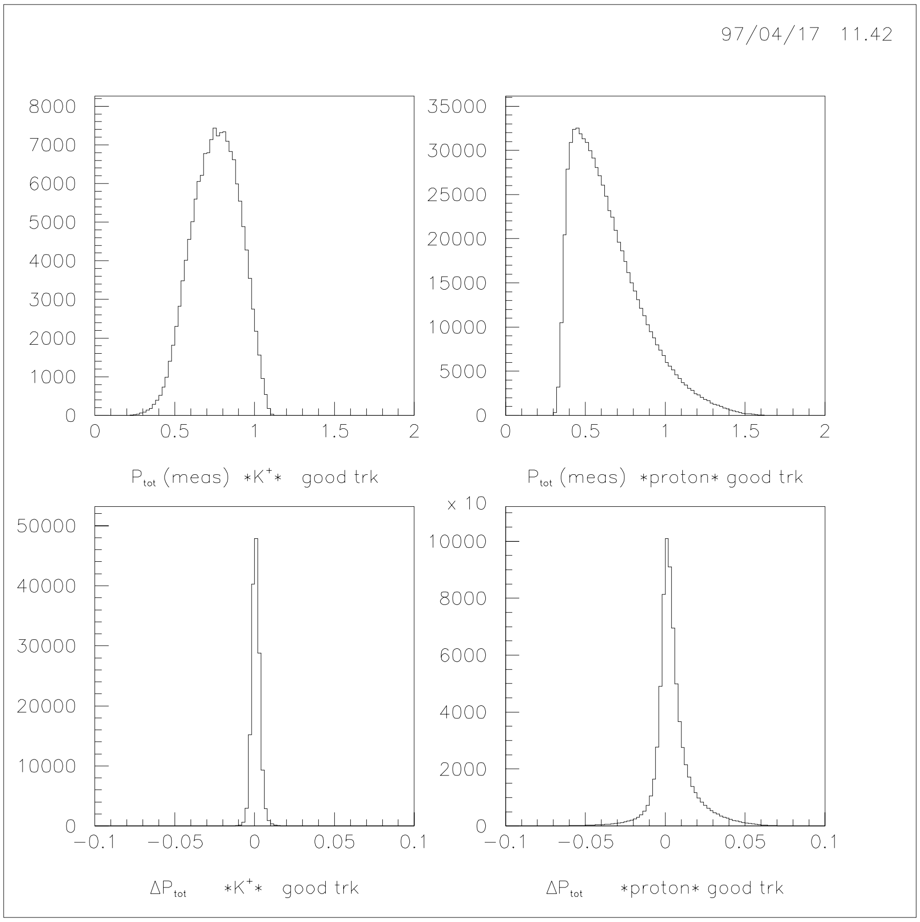

Figure 19: Detected Kaon and proton momenta (upper) and their corresponding relative uncertainties (lower).

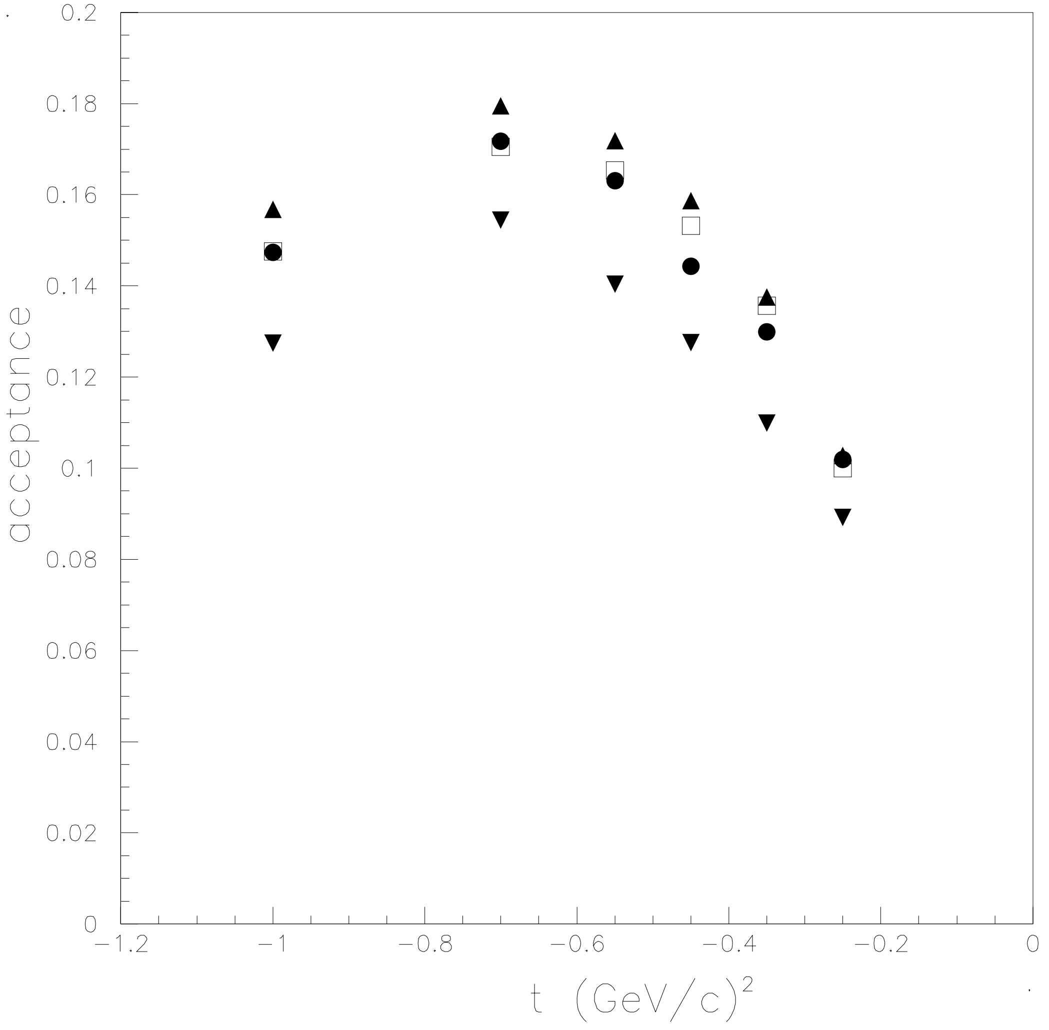

Figure 20: Acceptance ($N_{\text{detected}}/N_{\text{generated}}$) as a function of t for full B-field (open square), half B-field (solid triangle), full-field K^+ SCHC distribution (solid circle), and half B-field with $\Lambda^*(1520)$ cut (inverted triangle).

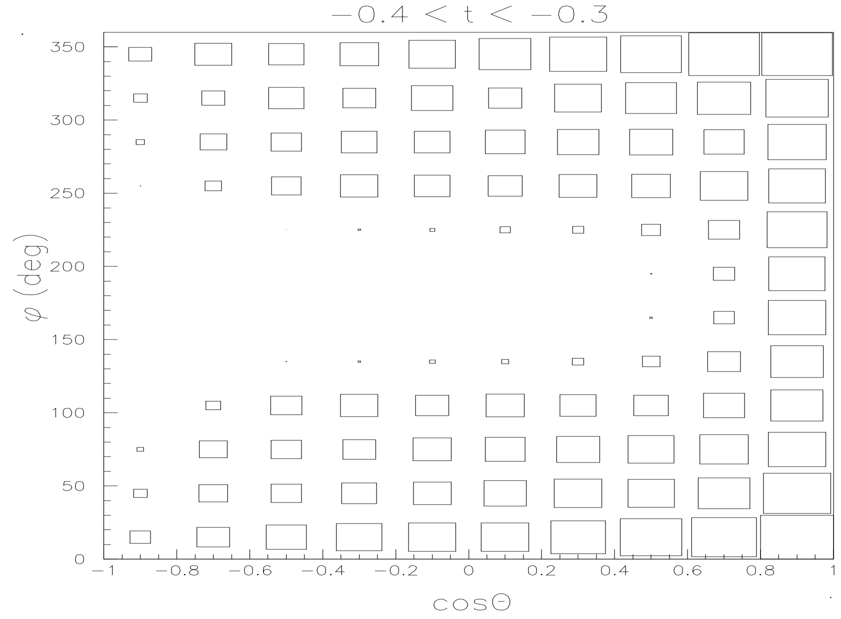

Figure 21: Acceptance ($N_{\text{detected}}/N_{\text{generated}}$) as a function of the K^+ decay angles in the helicity system for $-.4 < t < -.3$ (GeV/c)^2.

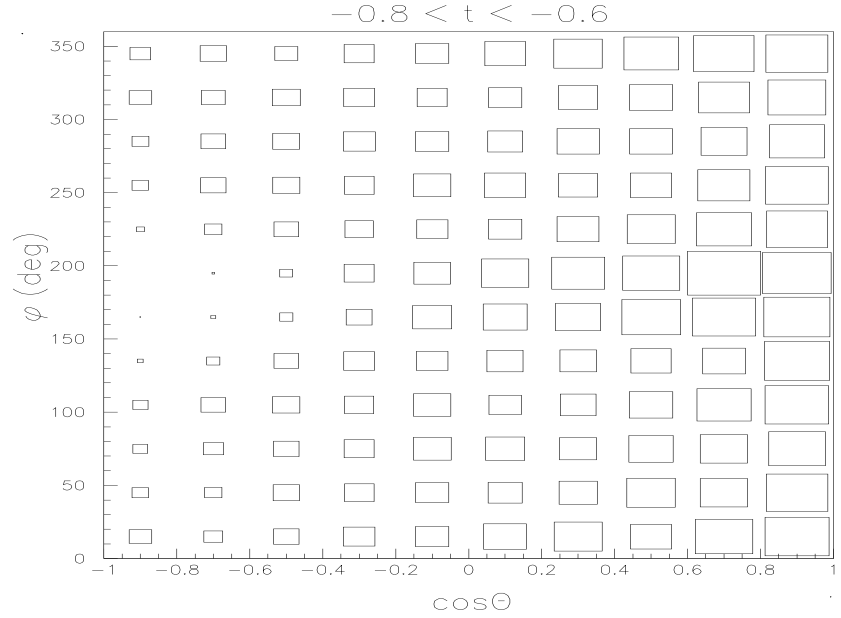

Figure 22: Acceptance ($N_{\text{detected}}/N_{\text{generated}}$) as a function of the K^+ decay angles in the helicity system for $-.8 < t < -.6$ (GeV/c)^2.

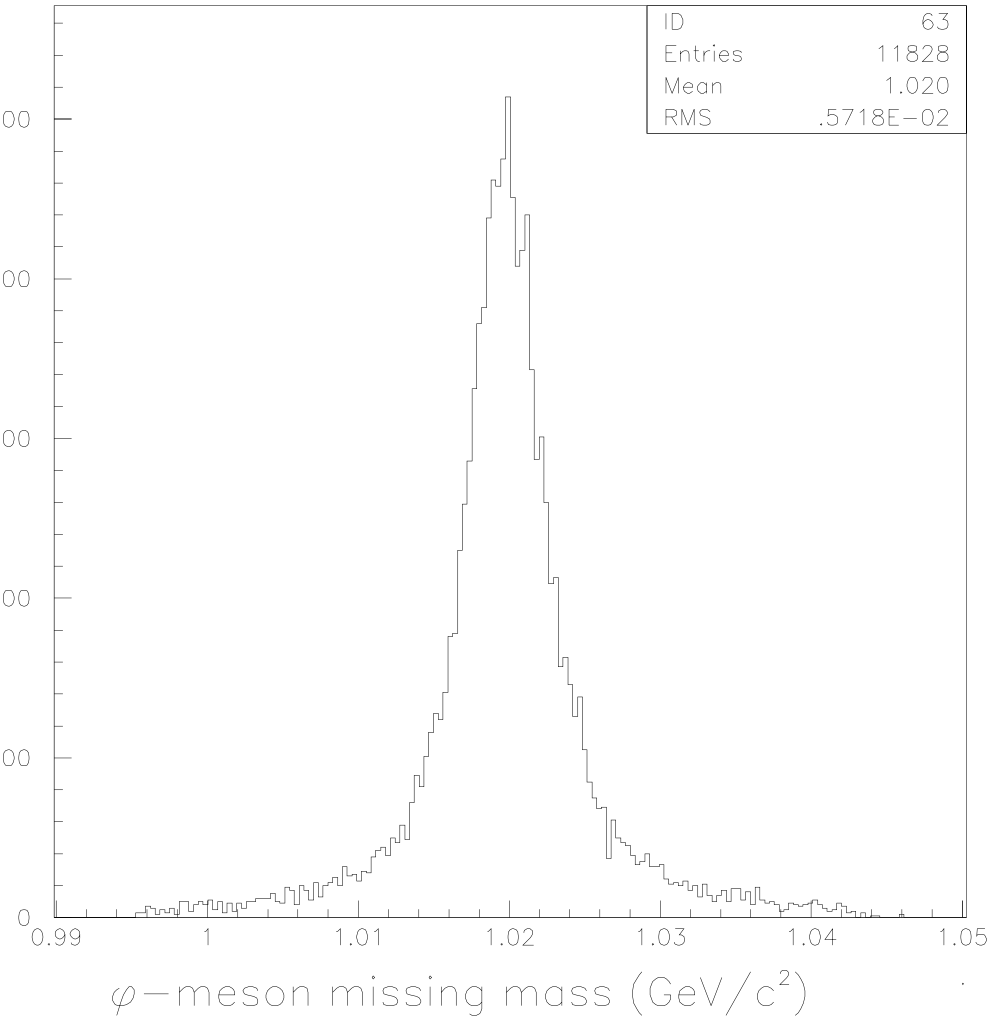

Figure 23: Reconstructed invariant mass of the ϕ meson.

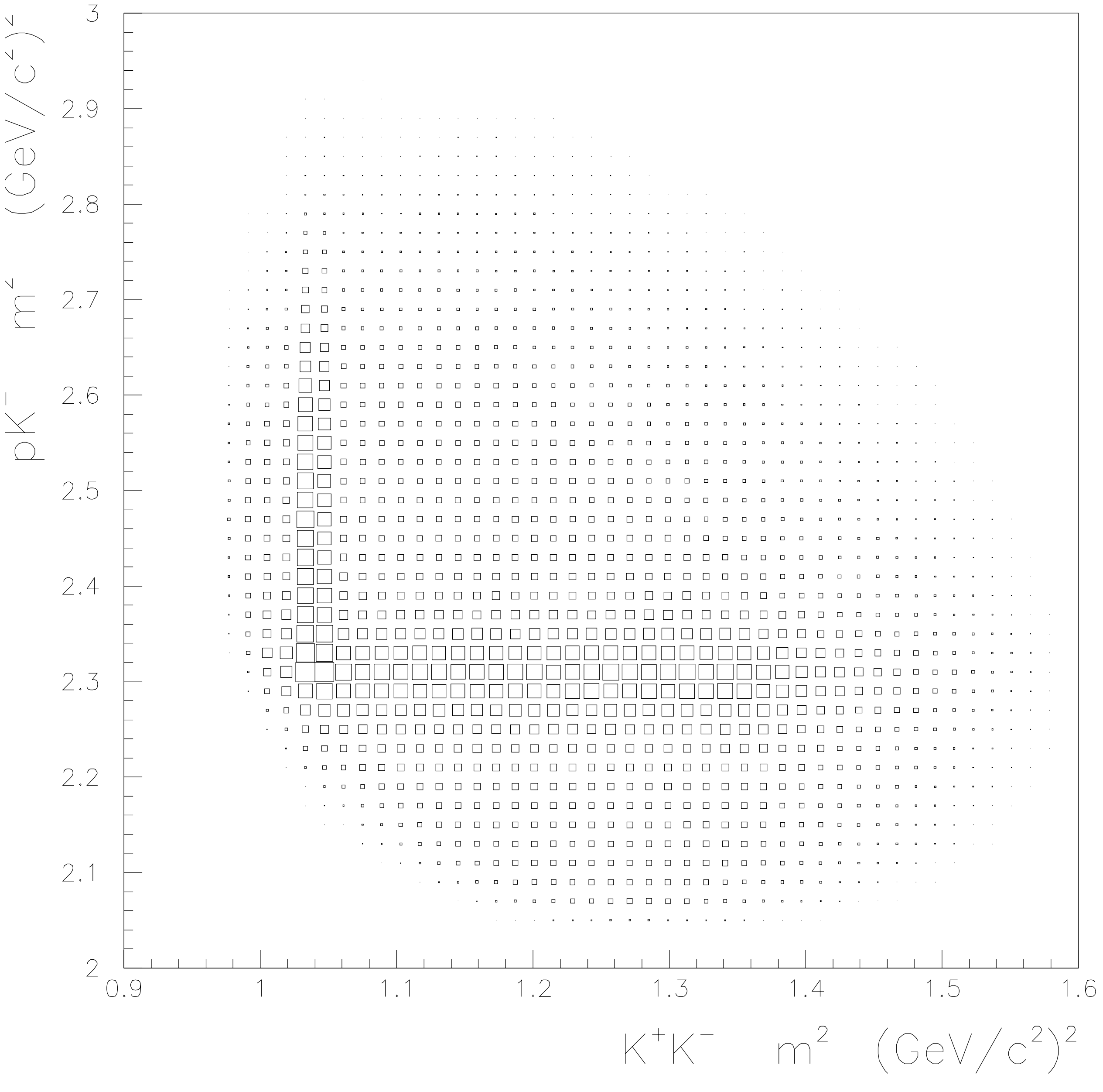

Figure 24: Dalitz plot containing contributions from ϕ meson, $\Lambda^*(1520)$, and s-wave K^+K^- production.

Figure 25: Missing mass spectrum from Reference [17].

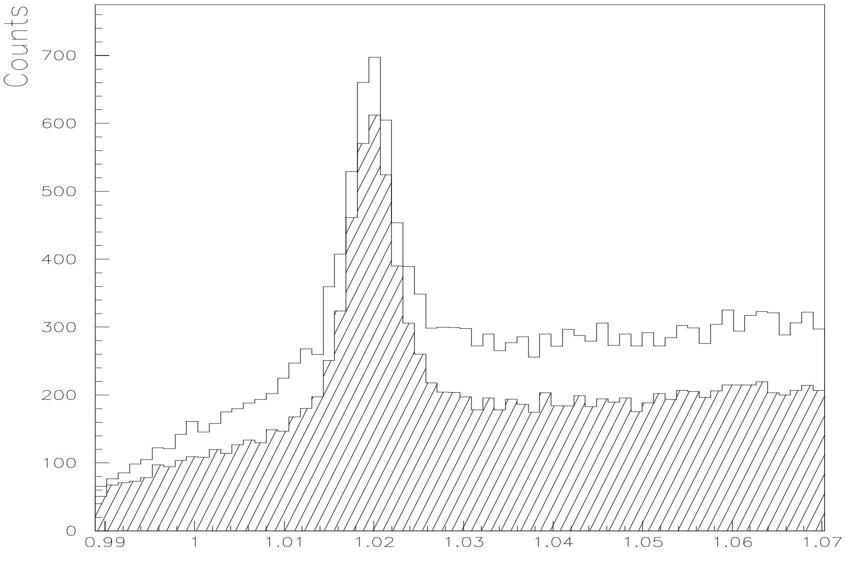

Figure 26: K^+K^- invariant mass for ϕ + s-wave + $\Lambda^*(1520)$ (total) and ϕ + s-wave K^+K^- (hatched).

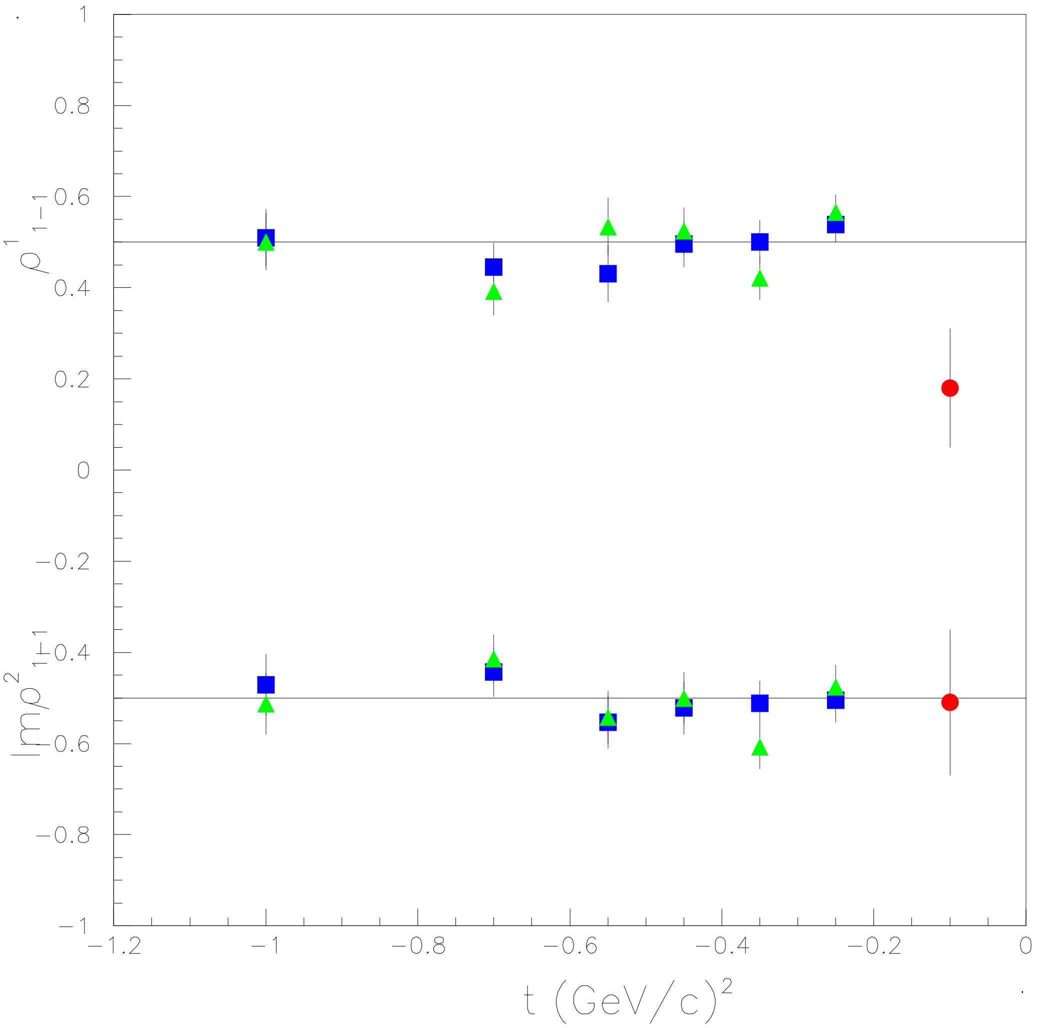

Figure 27: Results from MINUIT for maximum likelihood fit. The solid lines indicate the values used in the event generator and the points are the extracted values from the fit. The squares are the results of fitting the simulated ϕ data without background and the triangles are obtained from the fit to the data with background. The solid circles are the Ballam [15] data for the lowest photon energy range. (See Table 4)